

DIRECT DRIVE FUSION ENERGY SHOCK IGNITION DESIGNS FOR SUB-MJ LASERS

Andrew J. Schmitt, J. W. Bates, S. P. Obenshain, and S. T. Zalesak
Plasma Physics Division, Naval Research Laboratory, Washington DC 20375
andrew.schmitt@nrl.navy.mil

D. E. Fyfe
LCP&FD, Naval Research Laboratory, Washington DC 20375

R. Betti
Fusion Science Center and Laboratory for Laser Energetics, University of Rochester, Rochester NY

New approaches in target design have increased the possibility that useful fusion power can be generated with sub-MJ lasers. We have performed many 1D and 2D simulations that examine the characteristics of target designs for sub-MJ lasers. These designs use the recently-proposed shock-ignition target scheme, which utilizes a separate high-intensity pulse to induce ignition. A promising feature of these designs is their significantly higher gains at lower energies (one dimensional (1D) gain ~ 100 at $E_{laser} \sim 250\text{kJ}$) than can be expected for the conventional central ignition scheme. The results of these simulations are shown and we discuss the implications for target fabrication and laser design. Of particular interest are the constraints on the target and laser from asymmetries due to target imperfections and laser imprint.

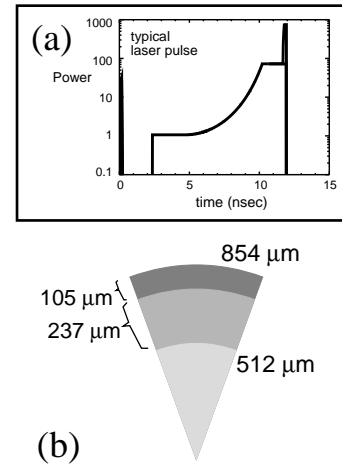


FIG. 1: The baseline target used in this study consists of a DT ice layer surrounded by an embedded low-density ($100\text{mg}/\text{cm}^3$) plastic foam layer. The target is driven by a short wavelength ($0.25\mu\text{m}$) KrF laser with a relaxation-type adiabat shaping pulse and uses two zooms (reductions of the laser spot dimensions during the implosion).

I. INTRODUCTION

Direct-drive laser inertial confinement fusion promises high gains for relatively modest laser energy. The conventional scheme involves directly illuminating a hollow DT sphere with some combination of laser beams, heating and ablating the exterior of the pellet, then compressing and accelerating it inwards to stagnation. The stagnation process creates an igniting hot spot and further compresses and burns the relatively cold fuel around it, leading to a release of fusion energy. In the past, the minimum drive energy needed to produce gains high enough for commercial applications of fusion power was thought to be of order of a few MJ¹⁻⁵. Recent research, however, has shown that sub-MJ laser drivers may also be useful on the path to practical fusion power.

A 500 kJ facility, called the Fusion Test Facility⁶ has been proposed to develop both the technology and the science of fusion power. This facility relies on the short wavelength KrF laser to produce the high drive pressures and implosion velocities necessary to ignite conventional direct-drive fusion targets while minimizing risk from hydrodynamic and laser plasma instabilities (LPI). Although not a high-gain facility projected to produce commercial fusion power, the expected gains from targets designed for this facility are high enough⁷ (gains ~ 50) to provide relevant engineering and physics proofs-of-principle for follow-on commercial applications. Recently, a new inertial fu-

sion scheme has been proposed⁸ that would enhance the utility of this kind of facility. This new concept is known as shock ignition, and it has the potential to produce even higher gains at this scale. Additionally, the unique capabilities required by this concept can best be provided with short wavelength, flexibly focused lasers like KrF drivers.

Shock ignition designs compress and accelerate the fuel in the conventional way, but do not produce implosion velocities high enough to ignite the target. Instead, a short spike of laser energy is used at the end of the pulse to launch a strong shock converging inward to the compressed core. This shock interacts with the outward going stagnation-driven shock to further compress and heat the core to ignition. The compression and the ignition of the pellet are thus separately controlled by the compression and the ignition pulses, and the freedom to optimize them separately allows the possibility of achieving higher gains. The capabilities needed by this concept, good light absorption and efficient laser-plasma coupling at very high intensities are enhanced by the high absorption efficiency and laser spot zooming provided by KrF.

Report Documentation Page

Form Approved
OMB No. 0704-0188

Public reporting burden for the collection of information is estimated to average 1 hour per response, including the time for reviewing instructions, searching existing data sources, gathering and maintaining the data needed, and completing and reviewing the collection of information. Send comments regarding this burden estimate or any other aspect of this collection of information, including suggestions for reducing this burden, to Washington Headquarters Services, Directorate for Information Operations and Reports, 1215 Jefferson Davis Highway, Suite 1204, Arlington VA 22202-4302. Respondents should be aware that notwithstanding any other provision of law, no person shall be subject to a penalty for failing to comply with a collection of information if it does not display a currently valid OMB control number.

1. REPORT DATE SEP 2008	2. REPORT TYPE	3. DATES COVERED 00-00-2008 to 00-00-2008			
4. TITLE AND SUBTITLE Direct Drive Fusion Energy Shock Ignition Designs for Sub-MJ Lasers		5a. CONTRACT NUMBER			
		5b. GRANT NUMBER			
		5c. PROGRAM ELEMENT NUMBER			
6. AUTHOR(S)		5d. PROJECT NUMBER			
		5e. TASK NUMBER			
		5f. WORK UNIT NUMBER			
7. PERFORMING ORGANIZATION NAME(S) AND ADDRESS(ES) Naval Research Laboratory, Plasma Physics Division, 4555 Overlook Avenue SW, Washington, DC, 20375		8. PERFORMING ORGANIZATION REPORT NUMBER			
9. SPONSORING/MONITORING AGENCY NAME(S) AND ADDRESS(ES)		10. SPONSOR/MONITOR'S ACRONYM(S)			
		11. SPONSOR/MONITOR'S REPORT NUMBER(S)			
12. DISTRIBUTION/AVAILABILITY STATEMENT Approved for public release; distribution unlimited					
13. SUPPLEMENTARY NOTES presented at the Technology of Fusion Energy conference, San Francisco CA, Sept. 2008, and is published in the American Nuclear Society Journal: Fusion Science and Technology 56, 377 (2009).					
14. ABSTRACT					
15. SUBJECT TERMS					
16. SECURITY CLASSIFICATION OF:			17. LIMITATION OF ABSTRACT Same as Report (SAR)	18. NUMBER OF PAGES 7	19a. NAME OF RESPONSIBLE PERSON
a. REPORT unclassified	b. ABSTRACT unclassified	c. THIS PAGE unclassified			

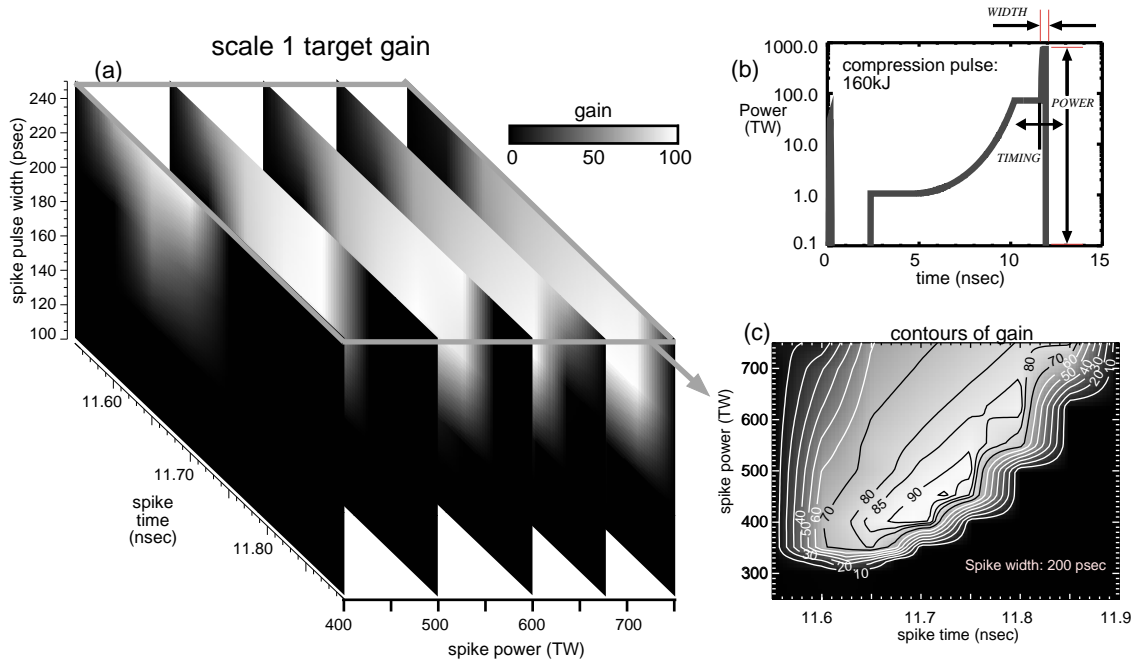


FIG. 2: (a) The gain varies as a function of spike ignitor timing, spike peak power, and spike FWHM pulse width, when using a compression power of 72.5 TW. The pulse shape is shown in (b), and (c) a slice of the data with spike width fixed at 200 psec, as a function of spike timing and power, shows peak gains near 100. The pulse compression power was also varied to produce a fourth dimension which is not shown here.

II. BASIC PELLET DESIGN

The target consists of a DT-ice inner core surrounded by an ablator made of low density (100 mg/cc) plastic foam into which liquid DT has been wicked up and frozen. The plastic foam serves as both a structural element for the target and increases the collisional absorption of the light. Because the compression pulse needn't accelerate the pellet to high velocities, the initial aspect ratio of the pellet can be rather small (~ 2.5). This provides more thickness for the incoming pellet shell to resist deterioration and breakup from the Rayleigh-Taylor instability. The baseline pellet for these studies is shown in Fig. 1. In actual manufacture, there will also be a thin CH layer encapsulating the pellet to provide a vapor barrier for the frozen DT within. This thin layer is ignored here to simplify the simulations; its presence is not expected to appreciably modify the results shown here. The laser pulse for this pellet was designed using the relaxation pulse ideas from Betti *et al.*⁹. This pulse is designed to provide tailoring of the pellet adiabat by impulsively shock heating the outside ablator and allowing it to decompress before applying the main pulse. This increases ablative stabilization of the Rayleigh-Taylor and Richtmyer-Meshkov instabilities and reduces the growth of short wavelength implosion asymmetries. The amplitude of the pulse foot, which produces a shock of about 3 Mbar, was chosen to put the inner fuel on a low adiabat. The amplitude of the main part of the compression pulse was initially chosen to produce an implosion velocity of about 2.5×10^7 cm/s, which is not enough to produce ignition by itself. We refer to the pulse without the ignition spike as the compression pulse.

The compression pulse is tuned by adjusting the power of the initial relaxation spike (it is Gaussian with a 1/e width of

50 psec), the turn-on time of the main pulse foot following the relaxation spike, and the time at which the peak compression power is achieved. This tuning is varied to produce the minimum fuel adiabat and highest compression as measured by peak density, pressure, and areal mass of the pellet. The resulting maximum intensity during the drive from the compression pulse alone is $\sim 2 \times 10^{15}$ W/cm². To efficiently use the laser energy, we “zoom” the laser spot twice during the laser pulse. It is zoomed first just as the main pulse hits maximum, and is reduced in size to the critical surface of the pellet at that time ($\sim 63\%$ of the original spot). The second zoom occurs just as the spike is turned on, and the reduction factor is again chosen to match the critical surface at that time ($\sim 41\%$ of original).

Once this tuning is achieved, an ignition spike is added to the pulse. The three parameters of the ignition spike – power, temporal width, and turn-on time (timing) – are studied by running many simulations with a systematic variation of those three parameters. A sample result is shown in Fig. 2, which shows slices from the resulting three-dimensional parameter space variation. In general, there is a range of spike timings that produce a close-to-optimal gain. At this point, the timing range (the range in spike timing that produces significant gain, ~ 100 psec for this target) increases with the peak spike power or its pulse width, both of which increase the energy going into the igniting shock. These 1D simulations predict that the maximum gain is near 100 when the laser energy is 250 kJ, of which 75 kJ is borne by the spike ignitor pulse. The ignitor spike power in this case is 450 TW over the 200 psec pulse width. Significant gain occurs when the spike has just enough energy to ignite the pellet (~ 350 TW); at this power level the spike timing can vary about ± 50 psec before the pellet fails to ignite. A more robust operating region can be attained by increasing the spike power.

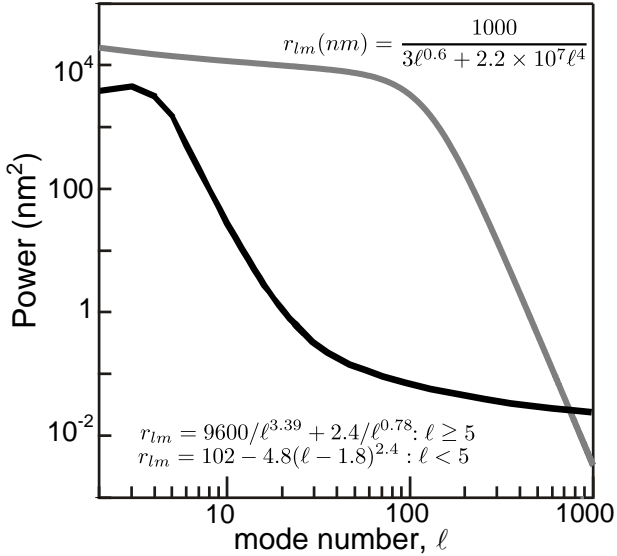


FIG. 3: The spectra of perturbations for the outer (black line) and inner (gray line) surface perturbations on the pellet. Note that the outer surface perturbations are highly peaked at the lowest mode numbers (longest wavelength). The formulas in the figure give the analytic formulae used for the mode amplitudes; the power spectra amplitude is $P_{2D} = (2\ell + 1)r_{\ell m}^2/4\pi$.

For instance, increasing the power to 600 TW doubles the extent of spike mistiming that is allowed (see Fig. 2c). This extra margin of power will also be useful to avoid sensitivity to other sources of imperfection, such as pellet surface perturbations or beam mispointing errors. For most of the two-dimensional (2D) sensitivity studies described later, we use a spike power of 750 TW, which is about twice the minimum ignitor power.

It is not obvious how much energy should be expended compressing the pellet versus igniting the pellet. We initially selected the compression power to be that which produced an implosion velocity of $2.5 \times 10^7 \text{ cm/s}$ without the ignitor spike. This is significantly less than the implosion velocity needed to trigger fusion without an ignitor spike (estimated to be $\approx 3.5 - 4 \times 10^7 \text{ cm/s}$). But is it the optimum? To answer this question, we also performed a parameter study with other compression powers while scanning the spike timing/spike power space (we fixed the FWHM of the spike at 200 ps here). The best gain is a mildly peaked function of the compression power near its absolute maximum, which was ~ 100 at 95 TW of compression power.

The spike powers used here can give rise to very large intensities in the pellet. These intensities can reach as high as $2 - 4 \times 10^{16} \text{ W/cm}^2$, which is well beyond the limit thought to be safe from deleterious laser plasma instabilities, even for the short wavelength ($0.25 \mu\text{m}$) light used here. However, this high intensity portion occurs only at the very end of the pulse, after significant compression has occurred due to both shocks and convergence effects. The areal mass of the pellet is rapidly rising (with a growth rate $\sim 350 \text{ psec}$) and varying between $\sim 0.05 - 0.1 \text{ g/cm}^2$ during the ignitor shock. This areal mass should be large enough to stop 100 keV electrons. Electrons of this order of magnitude in energy can be produced by laser

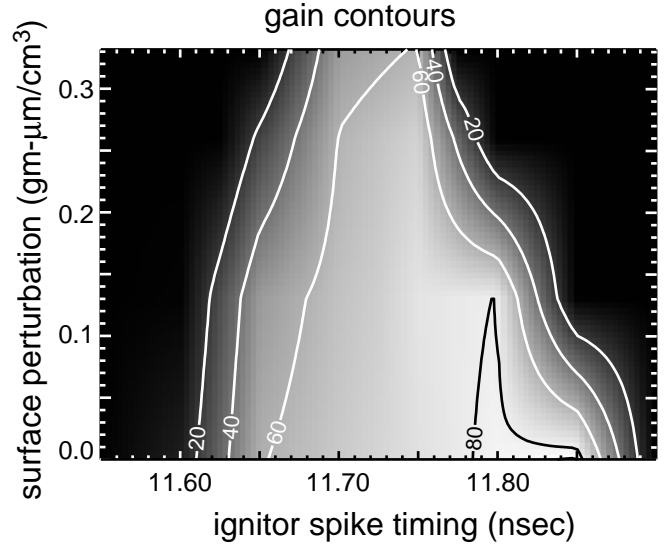


FIG. 4: The gain of the scale 1 target as a function of ignitor spike timing and power as predicted by low mode ($\ell < 16$) simulations. For comparison, the nominal “NIF-spec” level is equivalent to $0.13 \text{ g-}\mu\text{m/cm}^3$.

plasma instabilities like the two-plasmon decay instability in the underdense plasma. However, it is currently unknown how energetic or plentiful the hot electrons will be from such instabilities. This is an active area of research¹⁰⁻¹², but beyond the scope of this paper.

III. TWO DIMENSIONAL PERTURBATIONS

The next question to be addressed is the sensitivity of the pellet to 2D perturbations. Such perturbations can produce hydrodynamic instabilities in the pellet which will reduce or spoil the yields. The first type of perturbation we consider is pellet outer surface finish imperfections. We use a slightly modified “NIF-spec” surface spectrum¹³ (Fig. 3), which assumes more controllable, smaller amplitudes for the lowest modes ($\ell \leq 4$), although the spectrum still contains $\sim 90\%$ of its power in the modes $\ell < 10$.

An initial 2D scoping study was done using many low mode simulations with the outer surface finish as the perturbation source. These simulations used 880 points in the radial direction and 64 points in the polar angle direction; thus only modes $\ell = 2 - 16$ are described with at least 8 points per mode. (The mode $\ell = 1$ is not initialized in the simulations). A spike power of 750 TW and pulse width of 250 psec was used. We varied both the amplitude of the perturbation and the final ignitor shock timing. The simulation results, shown in Fig. 4, show that the pellet can survive outer surface pellet perturbations of $\sim \frac{1}{3} \text{ g-}\mu\text{m/cm}^3$ amplitude rms, albeit with reduced gain and higher sensitivity to ignitor spike timing. (For comparison, the “NIF-spec” amplitude is taken to be $0.13 \text{ g-}\mu\text{m/cm}^3$ rms ($\ell = 2 - 2000$) which is $\sim 0.125 \mu\text{m}$ rms in CH plastic, or $0.49 \mu\text{m}$ rms in the frozen, wetted CH foam ablator).

These low-mode simulations allow us to assess the influence of the secularly growing low-mode perturbations, but do

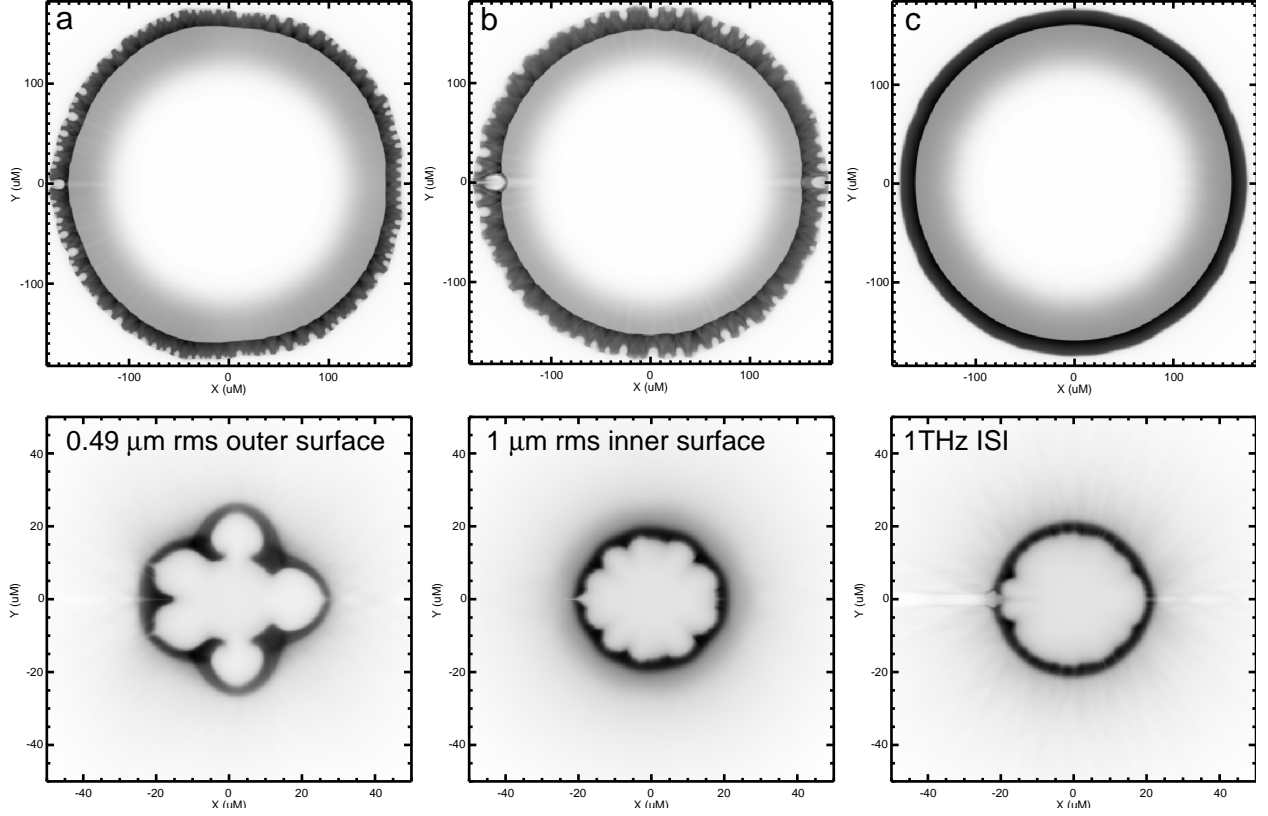


FIG. 5: For the scale 1 target, the density is shown at a two times during the implosion, and for three different scenarios. The upper images are at 12.05 nsec, after the ignition shock has been launched and just before shell deceleration, and the lower images are just as the burn begins ($t \sim 12.4 \text{ nsec}$). (Note different scales for upper / lower images). The three cases are for different applied perturbations: (a) outer surface; (b) inner surface; and (c) ISI laser imprint (300 overlapped beamlets). The 2D gains for these cases are (a) 60; (b) 78; and (c) 69.

not address the important issue of smaller wavelengths which can grow exponentially and more rapidly due to the Rayleigh-Taylor instability. Traditionally, these modes are the most dangerous and worrisome perturbations for direct drive because their amplification factor can peak at 5-6 e-foldings for $\ell \sim 100 - 200$.⁴ The targets here are different because they have a very low aspect ratio, are driven to relatively low velocities, and are therefore expected to be less sensitive to these instabilities. However, the omission of higher modes also neglects the effects of low-mode coupling to higher spatial frequencies.

To address the stability of the pellet to these high-frequency perturbations, we also ran high resolution simulations. We use 2048 points from pole-to-pole to resolve modes from $\ell = 1 - 512$ with at least 8 points per wavelength. Again, the $\ell = 1$ mode is not seeded. The perturbations due to outer surface perturbations, inner surface perturbations, and laser imprint from optical smoothing were simulated separately to determine their relative contributions. Fig. 5 shows images of the pellet density just before deceleration and near burn for each of these perturbations. All sources initially had a “nominal” amplitude – the outer surface was $0.488 \mu\text{m}$ rms (in the DT-wetted-foam), the inner surface was $1 \mu\text{m}$ rms, and the ISI driven perturbations were driven by 300 overlapped independent 1 THz ISI beams. Although all of them achieved a large fraction of the 1D gain, the outer surface perturbations lead to much larger perturbations than the other two sources. In addition, for outer surface de-

fects, the dominant structure as the pellet starts to burn is very low mode ($\ell \sim 5$), as seen in the Fig. 5a lower image. The high frequency mode growth has been suppressed both by ablative stabilization, the relatively short distance that the pellet shell accelerates, and the shell thickness (due to the small aspect ratio). The high frequency growth is thus not dominant (see Fig. 5 upper images, which are at times just before deceleration begins), and does not cause significant perturbations to the pellet. Of these three sources, the outer surface imperfections clearly result in the largest distortions in these targets.

There are a few reasons for the dominance of the outer surface perturbations in these simulations. First, the outer surface seed perturbations are fully formed at $t = 0$ (unlike the laser imprint). Second, they are acted upon immediately by the laser pulse (unlike the inner surface perturbations, which do not change until the first shock hits them, and do not cause significant growth until they can feed-out to the front surface where the Rayleigh-Taylor instability is active)¹⁴. Third, the bulk of these perturbations are initially low mode (the spectra of both the inner surface and ISI imprint are much broader bandwidth, and not concentrated into a small band, c.f. Fig. 3).

Why are low-mode perturbations so clearly dominant during the ignition and burn of the pellet? Some of this is because the high-mode perturbations have been effectively suppressed by the ablative stabilization, and have had limited growth because the fuel shell accelerates only a small distance inwards

TABLE I: Target specifications, listed by relative mass. In all cases, the ablator is made of $100\text{mg}/\text{cm}^3$ CH foam wicked with DT and frozen, the fuel layer is pure DT ice. The simulation parameters listed are those found in the case of the highest gain.

Scale (relative mass)	1×	2×	5×	8×
Outer Radius (μm)	854	1076	1455	1708
Ablator Thickness (μm)	108	136	177	216
Fuel Thickness (μm)	237	300	407	476
Best gain	101	143	210	243
E_{laser} (kJ)	231	398	727	1074
Absorption (%)	80	84	87	91
IFAR	21	20	16	14
ρR (g/cm^3)	2.4	2.9	3.4	3.4
Spike power (TW)	300	500	450	500
Spike pulse width (ps)	250	250	500	450
Compression power (TW)	95	110	120	160
<adiabat>	2.0	2.0	1.9	1.7
$V_{\text{implosion}}$ ($\times 10^7 \text{cm}/\text{s}$)	2.8	2.6	2.2	2.2
Spike energy ($E_{\text{spike}}/E_{\text{laser}}$)	0.18	0.20	0.21	0.13

(i.e., it has a low aspect ratio). However, it could also be expected that this pellet is sensitive to low-mode perturbations by simply noting the dimensions of the igniting hot spot (low density area in the middle of the pellet) in the lower images of Fig. 5. Those hot-spot sizes have a radius of about $20 \mu\text{m}$; with the starting outer radius of $854 \mu\text{m}$, this is a convergence ratio of about 43. This high convergence ratio means that the incoming shell must hit a smaller target (the hot spot) and thus has a smaller margin of aiming error. The aiming error is determined by the low-mode asymmetry.

It is not clear if this sensitivity to low modes can be easily removed from these designs, since the small hot spot is needed to minimize laser energy. An important advantage of shock ignition depends upon the ability to achieve higher gain by expending less energy in the ignitor than in conventional central ignition inertial fusion. Since the ignition energy varies as the ignitor mass ($\rho R_{\text{hot-spot}}^3$) with the constraint that alpha particle self-trapping occur ($\rho R_{\text{hot-spot}} \sim 0.3\text{g}/\text{cm}^2$), the ignitor energy varies as $R_{\text{hot-spot}}^2$ and a small (dense) hot spot is always needed for high gains. Decreasing the convergence ratio to lessen low-mode sensitivity would lead to using more driver energy to ignite the pellet. It is no coincidence that fast ignition designs share the same requirement for very small hot-spot dimensions.

The constraints on surface perturbations have been tested by simulating larger initial perturbation amplitudes. These simulations are ongoing, but we can report that the inner surface perturbation level can be as much as $3 \mu\text{m}$ rms and still not produce enough asymmetry to significantly destroy the high gain of this target (the gain drops to 68 at $3 \mu\text{m}$ rms from 78 at $1 \mu\text{m}$ rms). However, doubling the level of outer perturbations to twice the NIF-spec ($0.27 \text{g} - \mu\text{m}/\text{cm}^3$) prevents the pellet from igniting. Although the ostensible reason is the larger low-order modes produced by the larger initial amplitude, the discrepancy of this result with the earlier low-mode studies (Fig. 4) implies that the added resolution of higher modes contributes to

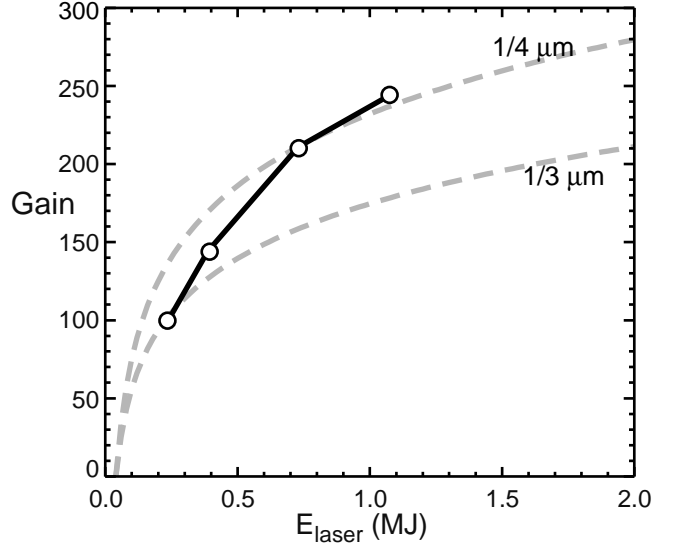


FIG. 6: The 1D best gain curve for the shock ignition targets simulated in this study. Shown for comparison (gray dashed lines) is the “maximum gain” for a $300 \text{g}/\text{cc}$ compressed fast ignition pellet¹⁵; the upper dashed curve corresponds to $0.25 \mu\text{m}$ and the lower curve to $0.35 \mu\text{m}$ laser wavelengths.

this failure. This result is still under study.

IV. ENERGY SCALING

The baseline pellet in Fig. 1 can be scaled up in mass by factors of 2, 5, and 8 to produce larger pellets at higher energies (Table I). The dimensions of each pellet are scaled by the cube root of the scale factor, and the pulse timings vary roughly by the same factor. For each pellet, a compression pulse is initially designed that keeps the fuel on a low adiabat and accelerates the target shell inward at about $2.5 \times 10^7 \text{cm}/\text{s}$. The intensity of the first foot is kept the same (the power scaling as $\text{mass}^{2/3}$). Again, we extensively search the spike timing/power/pulse-width space to determine a maximum gain, along with another search (usually at a single representative pulse width) while varying the compression pulse peak power. The results here summarize the output of a few thousand 1D runs that were done over all the scales and energies. Qualitatively, the behavior is quite similar to the results described for the baseline target. Quantitatively, the most significant parameter to change is the gain of the target. The gain curve giving the best gain cases is plotted in Fig 6, and the results are summarized in Table I.

To put these results in context, we compare the gains to those projected for fast ignition (FI). FI is another inertial fusion concept that takes advantage of the separation of pellet compression and ignition to minimize the energy involved in ignition and to produce higher gains. In FI, the compression phase is the same as in the shock ignition approach; the difference is that the ignition occurs through an intense focused beam of high-energy particles instead of shock heating. It is thus natural to wonder how these concepts compare. For comparison purposes, the shock ignition gain in Fig. 6 is plotted along with fast-ignition gain estimates from Eqn. (10) in the paper by Betti *et al.*¹⁵. This

TABLE II: Comparison of the scale 1 target design driven by KrF (0.25 μm wavelength) light, Nd:Glass (frequency tripled 0.35 μm wavelength) light, and Nd:Glass light without zooming. The “compress. only” columns refer to the parameters of the design when the ignitor spike is removed.

	KrF 0.25 μm zoom		glass 0.35 μm zoom		glass 0.35 μm no zoom	
	compress only	w/spike ignitor	compress only	w/spike ignitor	compress only	w/spike ignitor
Energy (kJ)	170	230	280	450	360	640
gain	–	92	–	55	–	33
absorption (%)	87	77	70	55	55	39
max. power (TW)	73	400	120	1000	220	1600
max. intensity ($\times 10^{15} W/cm^2$)	2.5	16	3.2	31	2.8	22
max. velocity ($\times 10^7 cm/s$)	2.5	2.8	2.5	2.8	2.5	2.8
max. $\rho R(g/cm^2)$	1.7	2.3	1.6	2.5	1.6	2.3

FI analysis predicts “maximum gain” curves for certain fast ignition directly-driven targets. The two curves in Fig. 6 show the theoretically expected maximum gain in a 300 g/cc isochoric fast ignition assembly directly compressed by either a 0.35 μm or 0.25 μm wavelength laser. (In that theoretical analysis, the ignitor energy is assumed to be negligible and laser zooming is not considered). The gains found here with the shock-ignition targets are comparable to the gain from those fast-ignition scenarios.

V. SHOCK IGNITION WITH ND:GLASS LASERS

We have also considered the use of a Nd:glass driver instead of the KrF laser driver. The shorter KrF wavelength has several advantages for the target physics: it allows higher absorption, drive pressure, mass ablation rate, and hydrodynamic efficiency than the longer wavelength glass laser. Also, the ability to zoom the laser spot during the implosion further maximizes the coupling; zooming is more difficult (although not impossible) for glass lasers. However, many of the laser facilities in the world are still based on Nd:glass drivers, so it is useful to look at the relative advantages and disadvantages of these features. (Other characteristics such as driver efficiency, optics complexity, and cost will also factor into driver wavelength comparisons, but they are not addressed here.)

The scale 1 target was taken as the baseline, and 1D simulations were used to examine the tradeoffs. There were two scenarios examined: the first changed the wavelength of the drive to 0.35 μm , and the second changed both the wavelength and also removed the ability of the laser to zoom. To produce a fair comparison, the glass laser drive was modified in both cases to produce as closely as possible the same drive pressure as the KrF laser, and thus should produce other parameters (e.g., compressed areal mass, shock timing, adiabat, and pellet yield) that are as similar as possible. Table II summarizes the results of the comparison. The energy penalty for the relatively small change in laser wavelength is considerable: almost twice as much energy is needed at the 0.35 μm wavelength, even allowing the glass laser to zoom. (It has been suggested that zooming may be accomplished with glass lasers, e.g. the French LMF facility,

by using different beams for the different zoom times. Although this is possible, it places additional restrictions on the use of the laser power.¹⁶⁾

Another concern with the longer laser wavelength is the higher maximum intensity that must be used to create the high pressures needed in shock ignition. This is due to both the decrease in hydrodynamic efficiency (the mean absorption density scales as $\sim \lambda^{-2}$) and the reduced absorption (the reduced density and the concomitant higher temperatures in the plasma corona give lower absorption). Very simply, LPI problems increase in severity when either the intensity or the laser wavelength is increased. A simple measure of the threat level is given by the product of the intensity and the square of the laser wavelength, $I\lambda^2$ (which is proportional to the nonlinear ponderomotive force that drives the LPI). This product is significantly higher for the glass laser scenarios, even during the compression phase of the laser drive when the target is much more sensitive to hot electrons. Consequently the glass laser designs may need lower intensities, and thus lower drive pressures and larger aspect ratio pellets. However, this would result in an increased risk of hydrodynamic instability.

VI. CONCLUSIONS

We have presented high-gain designs for direct-drive inertial fusion pellets at energies of 0.2 - 1.2 MJ, based on the recently proposed shock ignition concept. These designs rely on the short-wavelength drive (0.25 μm) of a KrF laser and on the ability to change the focal spot size by a factor of about two during the implosion. These features allow efficient coupling of the laser energy to the pellet and minimize the laser energy needed to achieve high gain.

Our results show that these targets have the potential to produce high gain, even with less than 500 kJ of drive energy. Extensive simulations, varying the spike power, spike pulse width, timing, and the compression power, were done to find the optimum conditions for the target ignition and gain. The requirements on the pulse intensity and sensitivity to pulse timing are within achievable ranges. Significant laser-plasma instabilities can be expected during the final high intensity ignitor spike, but

it is currently unknown whether this will be helpful or harmful.

Two dimensional simulations indicate that target robustness shrinks as the perturbation levels are increased, as expected. The simulations also indicate that neither the inner surface perturbation levels nor the laser imprint appears to be the major constraining factor in these designs. Instead, given the expected surface finish spectra, the outer surface perturbations are the dominant source in constraining the gain. Each perturbation source, considered individually and at its nominally achievable level, produces only modest gain degradation in the target. Simulations are underway to determine the limits on these sources, and to assess the behavior when they act together.

The sensitivity to the low-mode-dominant outer surface spectra, along with the relatively high convergence ratios that

are characteristic of these low energy designs, indicate that other low-mode asymmetries (e.g., beam configuration, power imbalance, and misaiming error) may also be important in determining the performance of these targets. These factors are currently under study.

ACKNOWLEDGMENTS

This work was supported by the U.S. Department of Energy. The authors wish to specifically thank Keith Obenschain for technical support of the cluster computing facilities.

-
- ¹ S. E. BODNER, D. G. COLOMBANT, J. H. GARDNER, R. H. LEHMBERG, S. P. OBENSCHAIN, L. PHILLIPS, A. J. SCHMITT, J. D. SETHAIN, R. K. MCCRORY, W. SEKA, C. VERDON, J. P. KNAUER, B. B. AFEYAN, and H. T. POWELL, *Phys. Plasmas* **5**, 1901 (1998).
 - ² A. J. SCHMITT, A. L. VELIKOVICH, J. H. GARDNER, C. PAWLEY, S. P. OBENSCHAIN, Y. AGLITSKIY and Y. CHAN, *Phys. Plasmas* **8**, 2287 (2001).
 - ³ P. W. MCKENTY, V. N. GONCHAROV, R. P. J. TOWN, S. SKUPSKY, R. BETTI, and R. L. MCCRORY, *Phys. Plasmas* **8**, 2315 (2001).
 - ⁴ A. J. SCHMITT, D. G. COLOMBANT, A. L. VELIKOVICH, S. T. ZALESKAK, J. H. GARDNER, D. E. FYFE, and N. METZLER, *Phys. Plasmas* **11**, 2716 (2004).
 - ⁵ B. CANAUD, X. FORTIN, F. GARAUDE, C. MEYER, F. PHILIPPE, M. TEMPORAL, S. ATZENI and A. SCHIAVI, *Nucl. Fusion* **44**, 1118 (2004).
 - ⁶ S.P. OBENSCHAIN, D. G. COLOMBANT, A. J. SCHMITT, J. D. SETHIAN, and M. W. MCGEOCH, *Phys. Plasmas* **13**, 056320 (2006).
 - ⁷ D. G. COLOMBANT, A. J. SCHMITT, S. P. OBENSCHAIN, S. T. ZALESKAK, A. L. VELIKOVICH, J. W. BATES, D. E. FYFE, J. H. GARDNER, and W. MANHEIMER, *Phys. Plasmas* **14**, 056317 (2007).
 - ⁸ R. BETTI, C. D. ZHOU, K. S. ANDERSON, L. J. PERKINS, W. THEOBALD, and A. A. SOLODOV, *Phys. Rev. Lett.* **98**, 155001 (2007); R. BETTI, W. THEOBALD, C. D. ZHOU, K. S. ANDERSON, P. W. MCKENTY, S. SKUPSKY, D. SHVARTS, V. N. GONCHAROV, J. A. DELETTREZ, P. B. RADHA, T. C. SANGSTER, C. STOECKL and D. D. MEYERHOFER, *J. Phys.: Conf. Ser.* **112**, 022024 (2008).
 - ⁹ K. ANDERSON and R. BETTI, *Phys. Plasmas* **10**, 4448 (2003); R. BETTI, K. ANDERSON, J. KNAUER, T. J. B. COLLINS, R. L. MCCRORY, P. W. MCKENTY, and S. SKUPSKY, *Phys. Plasmas* **12**, 042703 (2005).
 - ¹⁰ J. L. WEAVER, J. OH, B. AFEYAN, L. PHILLIPS, J. SEELY, U. FELDMAN, C. BROWN, M. KARASIK, V. SERLIN, Y. AGLITSKIY, A. N. MOSTOVYCH, G. HOLLAND, S. OBENSCHAIN, L-Y. CHAN, D. KEHNE, R. H. LEHMBERG, A. J. SCHMITT, D. COLOMBANT, and A. VELIKOVICH, *Phys. Plasmas* **14**, 056316 (2007).
 - ¹¹ B. YAAKOBI, C. STOECKL, W. SEKA, J. A. DELETTREZ, T. C. SANGSTER, and D. D. MEYERHOFER, *Phys. Plasmas* **13**, 062703 (2005).
 - ¹² C. STOECKL, R. E. BAHR, B. YAAKOBI, W. SEKA, S. P. REGAN, R. S. CRAXTON, J. A. DELETTREZ, R. W. SHORT, J. MYATT, and A. V. MAXIMOV, *Phys. Rev. Lett.* **90**, 235003 (2003).
 - ¹³ A. I. NIKITENKO, S. M. TOLOKONNIKOV, and R. COOK, *Fusion Tech.* **31**, 388 (1997); A. NIKROO, J. BOUSQUET, R. COOK, B.W. MCQUILLAN, R. PAGUIO, and M. TAKAGI, *Fusion Sci. Tech.* **45**, 165 (2004).
 - ¹⁴ A. L. VELIKOVICH, A. J. SCHMITT, J. H. GARDNER, and N. METZLER, *Phys. Plasmas* **8**, 592 (2001).
 - ¹⁵ R. BETTI, A. A. SOLODOV, J. A. DELETTREZ, and C. ZHOU, *Phys. Plasmas* **13**, 100703 (2006).
 - ¹⁶ B. CANAUD and F. GARAUDE, *Nucl. Fusion* **45**, L43 (2005).